

# Non-Extreme Individual Minima for Improved Pareto Front Sampling Efficiency and Decision-Making

Markus Herrmann-Wicklmayr

Kathrin Flaßkamp

Systems Modeling and Simulation, Saarland University, Saarbrücken, Germany  
`{markus.herrmannwicklmayr,kathrin.flasskamp}@uni-saarland.de`

## Abstract

In multi-objective optimization, the set of optimal trade-offs—the Pareto front—often contains regions that are extremely steep or flat. The Pareto optimal points in these regions are typically of limited interest for decision-making, as the marginal rate of substitution is extreme: a marginal improvement in one objective necessitates a significant deterioration in at least one other objective. These unfavorable trade-offs frequently occur near the individual minima, where single objectives attain their minimum values without considering the remaining criteria.

To address this, we propose the concept of *non-extreme individual minima* that relies on the notion of  $L$ -practical proper efficiency. These points can serve as a less sensitive replacement for *standard* individual minima in subsequent related methods. Specifically, they allow for a more practical restriction of the Pareto front sampling within a refined utopia-nadir hyperbox, provide a meaningful basis for image space normalization, and can enhance decision-making techniques, such as knee-point methods, by focusing on regions with acceptable trade-offs.

We provide a computationally efficient algorithm to determine these non-extreme individual minima by solving at most  $2n_J$  standard weighted-sum scalarizations, where  $n_J$  is the number of objectives. To ensure robustness across varying objective scales, the method incorporates an integrated image space normalization strategy. Numerical examples, specifically a convex academic case and a non-convex real-world application, demonstrate that the method successfully excludes practically irrelevant regions in the image space.

**Keywords:** Multi-objective optimization · Practical proper efficiency · Individual minima

## 1 Introduction

In multi-objective optimization problems (MOOPs), a solution is typically selected among all optimal trade-offs [13], i.e. the Pareto optimal points forming the so-called Pareto front (PF). This task must be performed either by a human decision-maker or by an automated decision-making scheme. In both cases, it

is reasonable to exclude parts of the PF that are extremely steep or flat, i.e. parts of the PF are avoided where a minor improvement in one objective yields a major deterioration in at least one other component. We denote the regions of the PF that are extremely steep or flat as *practically irrelevant*.

Conventionally, the identification of *relevant* solutions is performed a-posteriori: a human decision-maker localizes preferred regions only after a fine and ideally uniform sampling of the PF has been generated, which is a challenging task in itself [6]. However, this manual procedure is severely limited by human perception; once the number of objectives exceeds three, the resulting data points become nearly impossible to visualize and interpret.

Furthermore, modern applications with real-time requirements often preclude human intervention entirely, making this a-posteriori approach infeasible even for low-dimensional problems. Such scenarios necessitate automated decision-making methods. If these methods are guided by information about the individual minima (IMs) [16, 2, 10], it becomes particularly reasonable to utilize more robust reference points.

To address these challenges, we propose an a-priori strategy based on the notion of  $L$ -practical proper efficiency. By utilizing what we denote as *non-extreme* IMs, we can delimit the search space before the full sampling process begins. The core idea is to specifically target and remove unpromising regions in the proximity of the “standard” IMs where the marginal rate of substitution (MRS) is excessively high. Since these non-extreme IMs can be determined efficiently by solving at most  $2n_J$  weighted-sum (WS) scalarizations, they enable a more focused allocation of computational resources by avoiding practically irrelevant trade-offs from the outset. Beyond computational efficiency, this approach provides automated decision-making schemes (as e.g. [12, 14]) with less sensitive and more representative reference points, which ultimately increases the reliability of the resulting selection.

The paper is organized as follows: In Section 2 we introduce the basic notation and definitions of MOOPs. Furthermore, we define the term non-extreme IM. In Section 3 we show an intuitive way to compute non-extreme IMs. The method is then summarized in an algorithm. In Section 4 we apply the method to an exemplary MOOP. Finally, the paper is concluded in Section 5.

**Notation.** We denote the standard basis of  $\mathbb{R}^n$  by  $\{e_1, \dots, e_n\}$ . For a vector  $v \in \mathbb{R}^n$ , the relations  $v = 0$  and  $v \geq 0$  are to be understood component-wise, i.e.,  $v_i = 0$  and  $v_i \geq 0$  for all  $i = 1, \dots, n$ . We use the operator  $\text{diag}(v)$ , which returns a diagonal matrix with  $v$  on its diagonal and the sign function  $\text{sign}(x)$ , defined as  $\text{sign}(x) = 1$  if  $x > 0$  and  $\text{sign}(x) = -1$  otherwise. Bold symbols  $\mathbf{0}$  and  $\mathbf{1}$  denote vectors of zeros and ones, respectively, with context-dependent dimensions.

## 2 Preliminaries

We repeat the problem setting and the characterization of important quantities in MOOPs from [10] in the next two subsections.

## 2.1 Problem Statement

Consider the MOOP

$$\min_{x \in \mathbf{X}} \mathcal{J}(x) \quad (\mathcal{P})$$

with the vector  $\mathcal{J}(x) := [J_1(x), \dots, J_{n_J}(x)]^\top$  of  $n_J$  objectives  $J_i : \mathbf{X} \rightarrow \mathbb{R}$ ,  $i = 1, \dots, n_J$ . The set  $\mathbf{X} \subseteq \mathbb{R}^{n_x}$  denotes the feasible set; a point  $x \in \mathbb{R}^{n_x}$  is feasible if  $x \in \mathbf{X}$ . The vector-valued minimization in  $(\mathcal{P})$  is clarified by definitions and conventions adopted from [15].

**Definition 1** (Pareto optimality, nondominance). A point  $x^* \in \mathbf{X}$  is an efficient or a Pareto optimal solution to the multi-objective optimization problem  $(\mathcal{P})$  if there does not exist any feasible  $x \in \mathbf{X}$  such that

$$\begin{aligned} J_i(x) &\leq J_i(x^*) \text{ for all } i \in \{1, \dots, n_J\} \text{ and} \\ J_k(x) &< J_k(x^*) \text{ for at least one } k \in \{1, \dots, n_J\}. \end{aligned}$$

The respective image value  $\mathcal{J}(x^*)$  is called nondominated. The set of all nondominated points is the nondominated set or Pareto front  $\mathbf{J}_P := \{\mathcal{J}(x) \mid x \in \mathbf{X}_P\}$ , with the Pareto set  $\mathbf{X}_P$  given by

$$\mathbf{X}_P := \arg \min_{x \in \mathbf{X}} \mathcal{J}(x) = \{x \in \mathbf{X} \mid x \text{ is a Pareto optimal solution to } (\mathcal{P})\}.$$

## 2.2 Characteristic Quantities

We derive characteristic quantities of an MOOP. We denote by  $x_i^*$ ,  $i = 1, \dots, n_J$  the individual minima (IMs), i.e. solutions to the single-objective optimization problem  $\min_{x \in \mathbf{X}} J_i(x)$ ,  $i = 1, \dots, n_J$ . Evaluating the full objective vector  $\mathcal{J}$  at all IM defines the pay-off matrix (see, e.g. [5])  $\Phi = [\mathcal{J}(x_1^*), \dots, \mathcal{J}(x_{n_J}^*)]$ .

**Definition 2** (Utopia and nadir point). The utopia point (UP)  $\mathcal{J}_{UP}$  is defined as the row-wise minimum of  $\Phi$ . We define the nadir point (NP)  $\mathcal{J}_{NP}$  as the row-wise maximum of  $\Phi$ .

Note that, in literature, it is sometimes further distinguished between pseudo NPs (as defined in Definition 2) and real NPs [5, Chapter 2.2].

**Definition 3** (Normalized image space). Let  $C_{NP,UP}$  denote the positive definite, diagonal matrix  $C_{NP,UP} := \text{diag}(\mathcal{J}_{NP} - \mathcal{J}_{UP})^{-1}$ . Then, the operation  $\tilde{\mathcal{J}}(x) = C_{NP,UP}(\mathcal{J} - \mathcal{J}_{UP})$  shifts and scales the image space, such that the PF is contained in the unit box (or hyperbox) spanned by the two points  $\mathbf{0}$  and  $\mathbf{1}$ . We call this a normalized image space. The bar accent indicates a quantity in that normalized image space, e.g.  $\tilde{\mathcal{J}}_{UP} = \mathbf{0}$  and  $\tilde{\mathcal{J}}_{NP} = \mathbf{1}$  are the UP and NP in that normalized space.

### 2.3 Non-Extreme Individual Minima

In order to define what we mean by *non-extreme IMs* we first look at the definition of proper efficiency:

**Definition 4** (Proper efficiency (in the sense of Geoffrion [7])). A feasible point  $x' \in \mathbf{X}$  is a properly efficient solution if it is efficient and if there exists some real number  $M > 0$  such that, for each  $i \in \{1, \dots, n_J\}$  and  $x \in \mathbf{X}$  satisfying  $J_i(x) < J_i(x')$ , there exists at least one  $j \in \{1, \dots, n_J\} \setminus i$  such that  $J_j(x') < J_j(x)$  and

$$\frac{J_i(x') - J_i(x)}{J_j(x) - J_j(x')} \leq M.$$

We can illustrate Definition 4 with an exemplary bi-objective optimization problem in Figure 1 where we investigate the proper efficiency of the solutions

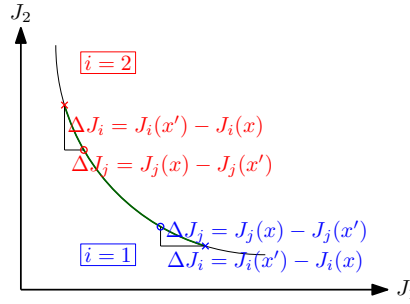


Figure 1: Objective value evaluated at  $x'$  marked with a cross, which was obtained using the weight vector  $w = (w_1, w_2)^\top$ , and at  $x$  marked with a circle.

$x'$  marked with a cross. For this it is helpful to consider a comparative solution  $x$ , marked with a circle. In the following we assume that  $w_i > 0, i \in \{1, \dots, n_J\}$ . We first fix the case where  $i = 2$  (and subsequently  $j$  must be 1). For a convex PF as in Figure 1 we know that at the solution  $\mathcal{J}(x')$ , that was obtained by solving the WS problem  $\min_{x \in \mathbf{X}} w^\top \mathcal{J}$ , the PF has the slope  $m = -w_1/w_2$ . We notice that with  $x \rightarrow x'$  the approximation

$$-w_1/w_2 = m \approx \frac{-(J_2(x') - J_2(x))}{J_1(x) - J_1(x')} =: \frac{-\Delta J_2}{\Delta J_1}$$

becomes exact. We then obtain  $w_1/w_2 = \lim_{x \rightarrow x'} \Delta J_2/\Delta J_1$ . In the same way, for the case  $i = 1$  (and  $j = 2$ ), we can derive  $w_2/w_1 = \lim_{x \rightarrow x'} \Delta J_1/\Delta J_2$ . This limit has a significant interpretation in multi-objective optimization: it represents the marginal rate of substitution (MRS). The MRS quantifies the rate at which a decision-maker is willing to sacrifice an amount of objective  $J_j$  to obtain a marginal improvement in objective  $J_i$  while remaining on the PF. In this context, the constant  $M$  in Definition 4 acts as an upper bound on the MRS. This means

that for both cases the solutions  $x'$  are properly efficient with  $M = w_1/w_2$  and  $M = w_2/w_1$ , respectively. For the general  $n_J$ -dimensional case, it was proved in [8, 11] that

$$\frac{J_i(x') - J_i(x)}{J_j(x) - J_j(x')} \leq \frac{w_j}{w_i}, \quad i, j \in \{1, \dots, n_J\}, i \neq j.$$

Although Definition 4 requires  $M$  to be finite, the value for it can still be arbitrarily high, implying an extreme trade-off where a negligible gain in one objective requires a massive loss in another. From an engineering or economic perspective, solutions with an excessively high MRS are not of practical relevance. In order to upper bound the value of  $M$  and thus the allowable MRS, we introduce the following definition:

**Definition 5** (*L*-practical proper efficiency). A feasible point  $x' \in \mathbf{X}$  is a *L*-practically properly efficient solution if it is properly efficient (as defined in Definition 4) with  $M \leq L$ .

We can now define the term non-extreme IM:

**Definition 6** (Non-extreme individual minimum). Let  $L > 0$ . We call a *L*-practically properly efficient solution  $\check{x}_i^*$  a non-extreme IM of the *i*-th objective if there exists no *L*-practically properly efficient solution  $x \in \mathbf{X} \setminus \check{x}_i^*$  such that  $J_i(x) < J_i(\check{x}_i^*)$ .

Note that we used a *breve* accent in order to differentiate between the *standard* IM  $x_i^*$  and the *non-extreme* IM  $\check{x}_i^*$ . We apply this notation to those quantities that exist in the standard and non-extreme case. An example of this notation is the non-extreme pay-off matrix

$$\check{\Phi} := \left[ \mathcal{J}(\check{x}_1^*), \quad \dots, \quad \mathcal{J}(\check{x}_{n_J}^*) \right]$$

which serves as the basis for deriving further quantities, such as the NP and UP.

## 2.4 Distance-Based Knee-Point

Based on the IM and the hyperplane spanned by their convex hull, [3] defines the knee-point as the point in the feasible image set  $\mathcal{J}(\mathbf{X})$  that maximizes the distance to this plane. Furthermore, in [4, 3] it was proved that the knee-point can be determined using either the WS scalarization with suitable weights. Since the knee-point is a point that is furthest to a hyperplane, this weight vector is the normal vector  $\eta$  of the considered hyperplane. However, the normal vector is only determined up to a non-zero constant. Since we want to avoid negative components in the weight vector, we define the following scaling operator.

**Definition 7** (Scaling vectors). Let the scaling operator  $\text{scal} : \mathbb{R}^n \setminus \{0\} \mapsto \mathbb{R}^n$  be defined such that for any  $v \in \mathbb{R}^n \setminus \{0\}$ , the output  $\tilde{v} = \text{scal}(v)$  is the unique vector  $\tilde{v} = cv$  with  $c \in \mathbb{R} \setminus \{0\}$  chosen to satisfy  $\text{sum}(|\tilde{v}|) = 1$  and  $\text{sign}(\tilde{v}_{i_{\max}}) = -1$ , where  $i_{\max} = \arg \max_i |\tilde{v}_i|$ .

Note that if the normal vector  $\eta$  has components with the same sign then the weight vector  $w_{\text{knee}} = \text{scal}(\eta)$  has only non-negative components. Similar to  $w_{\text{knee}}$  based on the standard IM, we can compute the  $\check{w}_{\text{knee}}$  based on the non-extreme IMs.

### 3 Computing Non-Extreme Individual Minima

#### 3.1 General Idea

The development of the method starts with recapitulating one approach to obtain a *standard*  $i$ -th IM. The approach uses the Pascoletti-Serafini scalarization [6, Chapter 2.1]

$$\begin{aligned} \min_{x \in \mathbf{X}, l \in \mathbb{R}} \quad & -l \\ \text{s.t.} \quad & \hat{\mathcal{J}}_{\text{SO}} + l\hat{d} - \tilde{\mathcal{J}}(x) \in \mathbf{K} \end{aligned} \tag{1}$$

that is parameterized in the shooting origin (SO)  $\hat{\mathcal{J}}_{\text{SO}}$  and the shooting direction vector  $\hat{d}$  and for which we choose

$$\begin{aligned} \mathbf{K} &= \left\{ \nu \in \mathbb{R}^{n_J-1} \mid -\hat{V}\nu \right\} \\ \text{and} \quad \tilde{\mathcal{J}}(x) &= \hat{T}_{\mathcal{J}}(\mathcal{J}(x) - \hat{\mathcal{J}}_{\text{shift}}). \end{aligned}$$

The parameters  $\hat{T}_{\mathcal{J}}$  and  $\hat{\mathcal{J}}_{\text{shift}}$  can be used to effectively transform and shift the image space. By appropriately setting these parameters the image space can be normalized.

In view of the different roles of the variables in this derivation, we adhere to a strict notation convention. While the *tilde* ( $\tilde{\cdot}$ ) is used flexibly for general modifications and transformations, the following three accents are reserved for specific contexts: the *hat* ( $\hat{\cdot}$ ) for parameter variables, the *check* ( $\check{\cdot}$ ) for their specific realizations, and the *breve* ( $\breve{\cdot}$ ) for quantities associated with the non-extreme case. Table 1 provides a summary of these conventions.

Accent	Example	Reserved meaning / use case
<i>hat</i>	$\hat{p}$	parameter of an optimization problem
<i>check</i>	$\check{p}$	numerical value of a parameter
<i>breve</i>	$\breve{\Phi}$	non-extreme case: quantities related to the non-extreme individual minima
<i>tilde</i>	$\tilde{\mathcal{J}}$	general modifications of a specific quantity

Table 1: Summary of mathematical notation conventions and reserved accents.

We solve (1) with the parameter realizations

$$\hat{T}_{\mathcal{J}} = I_{n_J}, \quad \hat{\mathcal{J}}_{\text{shift}} = \mathbf{0} \tag{3a}$$

$$\check{\mathcal{J}}_{\text{SO}} \in \mathbb{R}^{n_J}, \quad \check{d} = -e_i, \quad \check{V} = S_i := [e_k]_{k \in \{1, \dots, n_J\} \setminus i} \tag{3b}$$

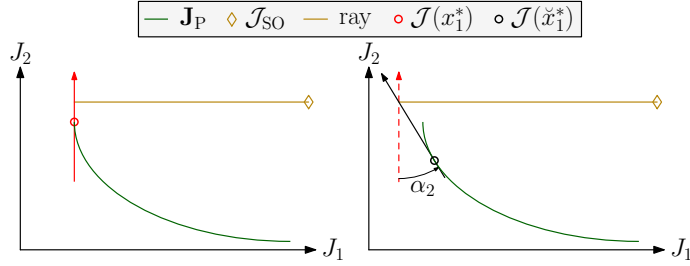


Figure 2: First individual minimum: standard approach (left) and non-extreme approach (right). The arrows represent the (elongated) vector  $S_2$  (red) and  $\tilde{S}_2(\alpha)$  (black).

to obtain the (standard)  $i$ -th IM. Equivalently, we can use the formulation

$$\begin{aligned} \min_{x \in \mathbf{X}, l \in \mathbb{R}, \nu \in \mathbb{R}^{n_J-1}} \quad & -l \\ \text{s.t.} \quad & \tilde{\mathcal{J}}(x) = \hat{\mathcal{J}}_{\text{SO}} + l\hat{d} + \hat{V}\nu. \end{aligned} \quad (P_{\text{PS}}(p))$$

with  $p = \{\hat{\mathcal{J}}_{\text{SO}}, \hat{d}, \hat{V}, \hat{T}_{\mathcal{J}}, \hat{\mathcal{J}}_{\text{shift}}\}$ . The optimization problem  $(P_{\text{PS}}(p))$  with the parameter realizations (3) can be understood and visualized as follows: A hyperplane, spanned by the column vectors of  $S_i$  (which we refer to as spanning vectors), is attached at the end of the shooting ray  $\hat{\mathcal{J}}_{\text{SO}} - le_i$ . A feasible objective vector  $\tilde{\mathcal{J}}(x)$  must then lie on that hyperplane.

We note that  $(P_{\text{PS}}(p))$  with  $\hat{d} = -e_i$  and  $\hat{V} = S_i$  is formally equivalent to the WS scalarization<sup>1</sup>

$$\min_{x \in \mathbf{X}} \hat{w}^\top \mathcal{J}(x) \quad (P_{\text{WS}}(\hat{w}))$$

with  $\tilde{w} = e_i$ . However, the application of the Pascoletti-Serafini scalarization provides a more convenient framework for the following derivation.

Instead of using basis vectors to span the hyperplane, we rotate each basis vector around a specific axis in a specific direction, see the exemplary rotation of  $e_2$  in Figure 2. The rotated spanning vectors read

$$\begin{aligned} v^{(i)}(\alpha_k) &= R_{n,m}(\text{sign}(k-i)\alpha_k) e_k, \\ i &\in \{1, \dots, n_J\}, \quad k \in \{1, \dots, n_J\} \setminus i, \end{aligned} \quad (4)$$

with  $n = \min\{k, i\}$ ,  $m = \max\{k, i\}$ ,  $\alpha = [\alpha_1, \dots, \alpha_{n_J}]$  and  $R_{n,m}(\phi)$  is a Givens rotation in the  $(n, m)$ -plane [9, chapter 5.1.8]. The Givens rotation  $R_{n,m}(\phi)$  is equal to the  $n_J \times n_J$  identity matrix except that the entries  $(n, n)$ ,  $(n, m)$ ,  $(m, n)$

<sup>1</sup>This formulation also covers the case of using  $\tilde{\mathcal{J}}$  instead of  $\mathcal{J}$ :  

$$\hat{w}^\top \tilde{\mathcal{J}} = \hat{w}^\top (\hat{T}_{\mathcal{J}}(\mathcal{J} - \hat{\mathcal{J}}_{\text{shift}})) = \underbrace{(\hat{T}_{\mathcal{J}}^\top \hat{w})^\top}_{=: \hat{w}'} \mathcal{J} - \underbrace{\hat{w}^\top \hat{\mathcal{J}}_{\text{shift}}}_{= \text{const.}}$$

and  $(m, m)$  are overwritten with

$$\begin{bmatrix} \cos(\phi) & -\sin(\phi) \\ \sin(\phi) & \cos(\phi) \end{bmatrix}.$$

The spanning vectors of our new hyperplane are concatenated horizontally to form

$$\check{S}_i(\alpha) = \left[ v^{(i)}(\alpha_k) \right]_{k \in \{1, \dots, n_J\} \setminus i}. \quad (5)$$

Note that  $\check{S}_i(\alpha) = S_i$  when  $\alpha = 0$ . Furthermore, the hyperplane associated with  $\check{S}_i(\alpha)$  has a normal vector  $w^{(i)}$  which we can scale such that  $w^{(i)} \geq 0$  and  $\sum_k w_k^{(i)} = 1$ .

Choosing  $\alpha > 0$ , we can now obtain the  $i$ -th non-extreme IM with  $(P_{\text{PS}}(p))$  by setting

$$\check{J}_{\text{SO}} \in \mathbb{R}^{n_J}, \quad \check{d} = -e_i, \quad \check{V} = \check{S}_i(\alpha) \quad (6)$$

and the remaining parameters as shown (3a) or with  $(P_{\text{WS}}(\hat{w}))$  by setting  $\check{w} = w^{(i)}$ . Choosing  $\alpha > 0$ , which yields  $w^{(i)} > 0$ , guarantees a finite  $L$  and thus also a non-extreme IM.

To see the general trend of increasing  $\alpha$  components we exemplarily set  $\alpha = \bar{\alpha}$ , with  $\bar{\alpha} \in \mathbb{R}_{>0}$  and compute

$$\bar{L} := \max_{i \in \{1, \dots, n_J\}} \max_{l, m \in \{1, \dots, n_J\}, l \neq m} w_l^{(i)} / w_m^{(i)}. \quad (7)$$

As we can see in Figure 3, with an increasing  $\bar{\alpha}$  the value of  $\bar{L}$  is strictly decreasing.

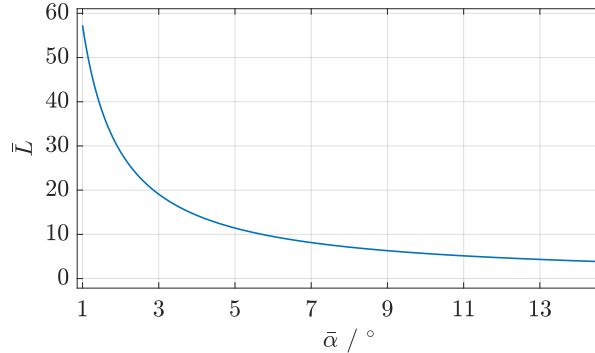


Figure 3: Finite values of  $\bar{L}$  for non-negative  $\bar{\alpha}$ .

Furthermore, numerical investigations show that  $\bar{L}$  seems to be invariant w.r.t. the number of objectives  $n_J$ .

### 3.2 Handling Different Objective Ranges

We apply the method to the exemplary three-objective optimization problem

$$\min_{x \in \mathbb{R}^3} \mathcal{J}(x) = \text{diag}([l_1, l_2, l_3])x \quad \text{s.t.} \quad x_1^2 + x_2^2 + x_3^2 \leq 1, \quad (8)$$

where the set of feasible objectives is a non-rotated ellipsoid with the semi-axis lengths  $[l_1, l_2, l_3]$ . For our investigations we choose  $\alpha = 10^\circ$ .

Our first numerical test uses the semi-axis lengths  $[l_1, l_2, l_3] = [1, 1, 1]$  (cf. Figure 4(a)) and we set the parameters as shown in (3a) and (6). Then, the method performs “as expected” in the sense that the set

$$\check{\mathbf{J}}_{\mathbf{P}} := \left\{ \mathcal{J} \in \mathbf{J}_{\mathbf{P}} \mid \mathcal{J} \leq \check{\mathcal{J}}_{\text{NP}} \right\}$$

excludes regions of the PF that we regard as practically irrelevant. However, in our second numerical test with  $[l_1, l_2, l_3] = [1, 3, 9]$  (cf. Figure 4(b)) and the parameter realizations as before the method fails to only exclude practically irrelevant regions.

To counteract this effect we can incorporate information about the NP and the UP which give us valuable insight over the ranges of the objectives. By choosing the parameter realizations

$$\check{I}_{\mathcal{J}} = C_{\text{NP,UP}}, \quad \check{\mathcal{J}}_{\text{shift}} = \mathcal{J}_{\text{UP}} \quad (9)$$

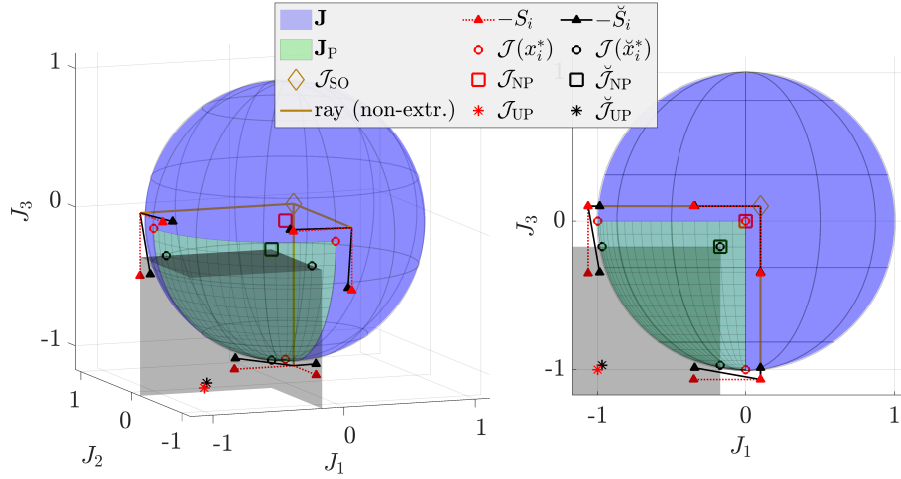
we normalize the image space. This idea of normalizing the image space also transfers to  $(P_{\text{WS}}(\hat{w}))$ . Here, we can realize the image space normalization by setting  $\tilde{w} = C_{\text{NP,UP}}^T w^{(i)} = C_{\text{NP,UP}} w^{(i)}$  instead of  $\tilde{w} = w^{(i)}$ .

The effect of the normalization approach is that (except for the shooting rays and the attached spanning vectors) the numerical results would produce a figure that looks like Figure 4(a) only that numbers on the  $J_2$  and  $J_3$  axis have changed to  $\pm 3$  and  $\pm 9$ . This means that  $\check{\mathbf{J}}_{\mathbf{P}}$  now contains the desired region of the PF.

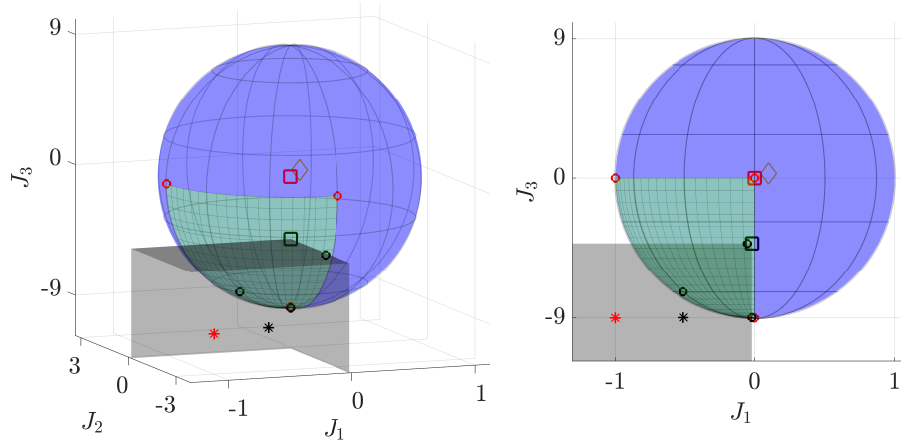
### 3.3 Algorithm

We can combine the previous findings to construct Algorithm 1. Notably, step 0) of this algorithm needs to be performed only once for a fixed  $\alpha$ . Furthermore, if the values of  $\mathcal{J}_{\text{NP}}$  and  $\mathcal{J}_{\text{UP}}$  are not available, which is generally the case, step 1) and 2) have to be executed. Then, in total,  $2n_J$  optimization problems have to be solved to determine the non-extreme IMs.

Applying Algorithm 1 to MOOP (8) with  $\alpha = \bar{\alpha}$ , where  $\bar{\alpha} = 0^\circ, 1^\circ, \dots, 10^\circ$ , yields Figure 5. While NP values of non-extreme IMs drop significantly, the associated UP values show only a slight increase. This effect yields hypercubes of reduced size which allow for a denser sampling of the PF with a fixed number of sampling points or, alternatively, fewer samples for a targeted approximate point density. By omitting practically irrelevant regions, improved resolution or efficiency gains are achieved.



(a) The semi-axis lengths are  $[l_1, l_2, l_3] = [1, 1, 1]$  and no image space normalization is used. Note that only the ray for the non-extreme case is displayed. For comparison, at the end of the rays both sets of spanning vectors are “attached”. Due to the symmetry the views in the other two planes look the same as the  $J_1$ - $J_3$ -plane on the right.



(b) The semi-axis lengths are  $[l_1, l_2, l_3] = [1, 3, 9]$  and no image space normalization is used. For reasons of a cleaner visual presentation, we refrain from displaying the spanning vectors and the shooting rays.

Figure 4: Results for the multi-objective optimization problem (8).

---

**Algorithm 1** Non-Extreme Individual Minima

---

- 0) Use  $\alpha$  to compute  $\check{S}_i(\alpha)$ ,  $i \in \{1, \dots, n_J\}$ . Then, compute  $w^{(i)}$  as the normal vector of the hyperplane spanned by the column vectors of  $\check{S}_i(\alpha)$  as defined in (5) and (4) (and scale it as described in Definition 7).
  - 1) Solve  $(P_{\text{WS}}(\hat{w}))$  with  $\check{w} = e_i$  for all  $i \in \{1, \dots, n_J\}$  and compute  $\Phi$ .
  - 2) Derive  $\mathcal{J}_{\text{NP}}$ ,  $\mathcal{J}_{\text{UP}}$  and  $C_{\text{NP,UP}}$  from  $\Phi$ .
  - 3) Solve  $(P_{\text{WS}}(\hat{w}))$  with  $\check{w} = C_{\text{NP,UP}}w^{(i)}$  for all  $i \in \{1, \dots, n_J\}$  and compute  $\check{\Phi}$ .
- 

## 4 Numerical Example

As our numerical example we consider the PF of “Figure 6.” from [10]. This reference describes in detail how the MOOP, which implements a nonlinear *heating, ventilation and air conditioning* control problem and yields the PF depicted in Figure 6 (left), is constructed. We choose this specific PF because i) it constitutes a non-academic example and ii) it has a large region where it is either extremely flat or steep.

We set  $\alpha = 3^\circ$  which results in  $L = \bar{L} < 20$  (cf. (7)) for the non-extreme IMs (cf. Figure 3). We then compute the standard IMs and the non-extreme IMs as described in Algorithm 1. Both resulting sets of points can be seen in Figure 6. As can be concluded from the closeness of  $\check{\mathcal{J}}_{\text{UP}}$  to  $\mathcal{J}_{\text{UP}}$  only extreme trade-off solutions are excluded. This is supported by the fact that Figure 6 (right) has no regions that are extremely flat or steep.

We note that from all 1520 PF samples shown in Figure 6 (left) only 186 are contained in the box spanned by  $\check{\mathcal{J}}_{\text{NP}}$  and  $\check{\mathcal{J}}_{\text{UP}}$ . This means that, since sampling practically irrelevant points on the PF provides no added value to the decision-maker, more than 87% of the optimizations represented a superfluous expenditure of time and resources that our method successfully eliminates. Furthermore, for Figure 6, the knee-points based on the standard and non-extreme IMs were computed. This requires the normal vector of the convex hull of the IMs and non-extreme IMs, which are  $w_{\text{knee}} = [-0.0239, 0.9673, -0.0088]^\top$  and  $\check{w}_{\text{knee}} = [0.0306, 0.9527, 0.0167]^\top$ , respectively. Note that  $w_{\text{knee}}$  contains negative components. This leads to two critical issues: first, the theoretical guarantee of obtaining a Pareto optimal solution is lost; second, and more importantly, the scalarization effectively rewards increases in cost for objectives associated with negative weights, contradicting the fundamental goal of minimization. Consequently, the resulting point  $\mathcal{J}_{\text{knee}} = 10^3 \cdot [2.9783, 0.0036, 3.1886]^\top$  is a dominated point located on the boundary of the feasible image set  $\mathcal{J}(\mathbf{X})$  and is outside the axis intervals of Figure 6. Enforcing a lower bound of zero on the weight components as a “safety layer” would, in this example, lead to the recovery

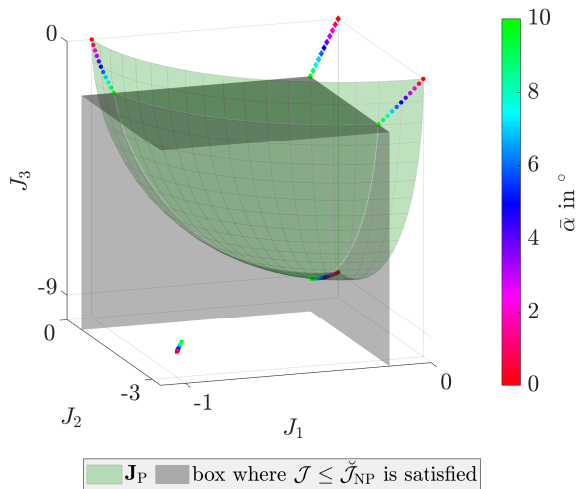


Figure 5: The colored markers are related to the non-extreme IMs (with  $\alpha = \bar{\alpha}$ ): dots represent the non-extreme IMs, while diamonds and squares represent the corresponding NPs and UPs, respectively.

of the second IM. However, such a solution contradicts the fundamental concept of a knee point, which is intended to represent a balanced compromise rather than an extreme boundary solution. In contrast, the solution  $\check{J}_{\text{knee}}$  obtained by using the weight  $\check{w}_{\text{knee}}$  (constructed from the non-extreme IMs) constitutes a balanced trade-off.

## 5 Conclusion and Outlook

In this paper, we introduced the concept of non-extreme individual minima as a means to exclude practically irrelevant regions of the Pareto front. By leveraging the definition of  $L$ -practical proper efficiency, we derived a method to exclude solution candidates that represent unreasonable trade-offs.

The proposed algorithm is straightforward to implement, relying solely on weighted-sum scalarizations with modified weight vectors obtained via geometric rotations. We demonstrated that integrating information about the utopia point and the nadir point to normalize the image space is crucial for the method's robustness against differing objective ranges. The numerical results confirm that the computed non-extreme individual minimum effectively bound the area of interest, excluding extremely steep or flat parts of the front. This bounding box allows subsequent multi-objective optimization methods or automated decision-making schemes to focus their computational effort on the most promising trade-offs.

Future work could evaluate the influence of this approach on algorithms that rely on automated decision-making. A prime example of this is the Pareto

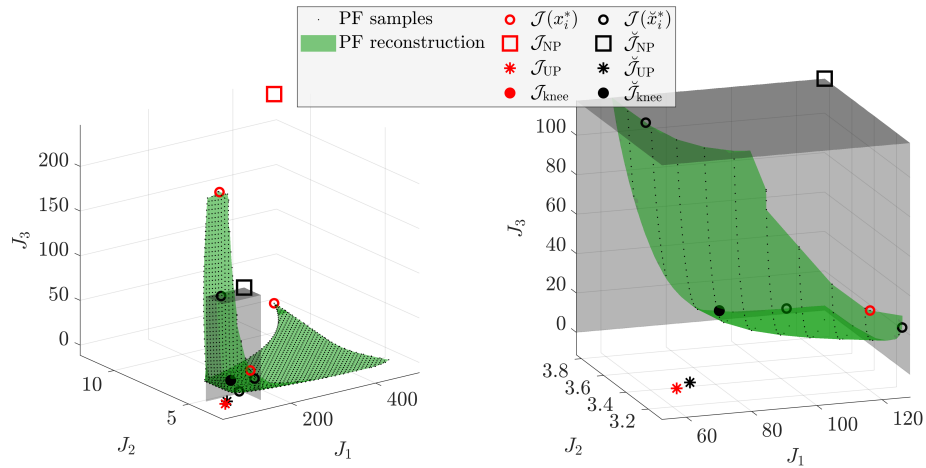


Figure 6: PF reconstruction using the PF samples and the ball-pivoting algorithm [1]. The right plot shows a segment of the PF that does not contain practically irrelevant regions. Both figures use an equal plot box aspect ratio which has a similar visual effect as normalizing the image space and allows for a fair comparison of both PF regions.

front from [10] shown in Figure 6, which arises during the first iteration of an multi-objective model predictive control scheme.

## References

- [1] F. Bernardini, J. Mittleman, H. Rushmeier, C. Silva, and G. Taubin. The Ball-Pivoting Algorithm for Surface Reconstruction. *IEEE Transactions on Visualization and Computer Graphics*, 5(4):349–359, October 1999. ISSN 1077-2626. URL <https://doi.org/10.1109/2945.817351>.
- [2] Wei-Yu Chiu, Gary G. Yen, and Teng-Kuei Juan. Minimum Manhattan Distance Approach to Multiple Criteria Decision Making in Multi-objective Optimization Problems. *IEEE Transactions on Evolutionary Computation*, 20(6):972–985, December 2016. ISSN 1941-0026. URL <https://doi.org/10.1109/TEVC.2016.2564158>.
- [3] I. Das. On characterizing the “knee” of the Pareto curve based on Normal-Boundary Intersection. *Structural optimization*, 18(2):107–115, October 1999. ISSN 1615-1488. URL <https://doi.org/10.1007/BF01195985>.
- [4] Indraneel Das and J. E. Dennis. Normal-Boundary Intersection: A New Method for Generating the Pareto Surface in Nonlinear Multicriteria Optimization Problems. *SIAM Journal on Optimization*,

- 8(3):631–657, August 1998. ISSN 1052-6234, 1095-7189. URL <https://doi.org/10.1137/S1052623496307510>.
- [5] Matthias Ehrgott. *Multicriteria Optimization*. Springer, Berlin, 2nd ed edition, 2005. ISBN 978-3-540-21398-7. URL <https://doi.org/10.1007/3-540-27659-9>.
- [6] Gabriele Eichfelder. *Adaptive Scalarization Methods in Multiobjective Optimization*. Vector Optimization. Springer Berlin, Berlin Heidelberg, 2008. ISBN 978-3-540-79157-7. URL <https://doi.org/10.1007/978-3-540-79159-1>.
- [7] Arthur M Geoffrion. Proper Efficiency and the Theory of Vector Maximization. *Journal of Mathematical Analysis and Applications*, 22(3):618–630, June 1968. ISSN 0022-247X. URL [https://doi.org/10.1016/0022-247X\(68\)90201-1](https://doi.org/10.1016/0022-247X(68)90201-1).
- [8] J. C. Geromel and P. A. Valente Ferreira. An upper bound on properly efficient solutions in multiobjective optimization. *Operations Research Letters*, 10(2):83–86, March 1991. ISSN 0167-6377. URL [https://doi.org/10.1016/0167-6377\(91\)90091-3](https://doi.org/10.1016/0167-6377(91)90091-3).
- [9] Gene H. Golub and Charles F. Van Loan. *Matrix Computations*. Johns Hopkins studies in the mathematical sciences. Johns Hopkins University Press, Baltimore, 3rd ed edition, 1996. ISBN 978-0-8018-5413-2 978-0-8018-5414-9. URL <https://doi.org/10.56021/9781421407944>.
- [10] Markus Herrmann-Wicklmayr and Kathrin Flaßkamp. Individual Minima-Informed Multi-Objective Model Predictive Control for Fixed Point Stabilization, October 2025. URL <http://arxiv.org/abs/2510.23454>.
- [11] Masoud Karimi and Balal Karimi. Linear and conic scalarizations for obtaining properly efficient solutions in multiobjective optimization. *Mathematical Sciences*, 11(4):319–325, December 2017. ISSN 2008-1359, 2251-7456. URL <https://doi.org/10.1007/s40096-017-0234-0>.
- [12] Wenhua Li, Guo Zhang, Tao Zhang, and Shengjun Huang. Knee Point-Guided Multiobjective Optimization Algorithm for Microgrid Dynamic Energy Management. *Complexity*, 2020:1–11, November 2020. ISSN 1099-0526, 1076-2787. URL <https://doi.org/10.1155/2020/8877008>.
- [13] Bernard Roy. *Multicriteria Methodology for Decision Aiding*, volume 12 of *Nonconvex Optimization and Its Applications*. Springer US, Boston, MA, 1996. ISBN 978-1-4419-4761-1 978-1-4757-2500-1. URL <https://doi.org/10.1007/978-1-4757-2500-1>.
- [14] Thomas Schmitt, Matthias Hoffmann, Tobias Rodemann, and Jürgen Adamy. Incorporating Human Preferences in Decision Making for

Dynamic Multi-Objective Optimization in Model Predictive Control. *Inventions*, 7(3):46, June 2022. ISSN 2411-5134. URL <https://doi.org/10.3390/inventions7030046>.

- [15] Marleen Stieler. *Performance Estimates for Scalar and Multiobjective Model Predictive Control Schemes*. PhD thesis, March 2018. URL <https://nbn-resolving.org/urn:nbn:de:bvb:703-epub-3783-4>.
- [16] Victor M. Zavala and Antonio Flores-Tlacuahuac. Stability of multiobjective predictive control: A utopia-tracking approach. *Automatica*, 48(10):2627–2632, October 2012. ISSN 00051098. URL <https://doi.org/10.1016/j.automatica.2012.06.066>.